

Space charge distribution in dielectric barrier discharge

J. Park and M. S. Cha

CCRC, Physical Science and Engineering Division (PSE), King Abdullah University of Science and Technology (KAUST), Thuwal, Saudi Arabia

Abstract: Space charges play an important role in a mechanism for microdischarges (MDs) in alternating current (AC) driven dielectric barrier discharges (DBDs). However, the growth and decay of the space charges have not been experimentally investigated. This study investigated the space charge by measuring an electric field using the electric-field-induced second harmonic generation (EFISH) technique. Experimental results successfully illustrated the development of the space charges in a two-dimensional (2D) domain.

Keywords: Dielectric barrier discharge (DBD), Microdischarge (MD), Space charge, Electric-field-induced second harmonic (EFISH) technique

1. Introduction

Dielectric Barrier Discharges (DBDs) have a long history, ever since Siemens developed an ozone generator in 1857 [1]. DBD is one of the typical non-thermal plasmas, operating under the wide range of gas temperature and pressure with a relatively simple structure (two electrodes and an insulator between electrodes). Thus, it has been used in various fields such as water treatment [2, 3], surface treatment [4–6], and plasma medicine [7, 8].

DBD at atmospheric pressure consists of microdischarges (MDs) lasting a few nanoseconds. MD filaments leave space charges behind, and these behave as seeds for the next generation of MD as the polarity of applied alternating current (AC) changes [9]. In this regard, many studies have shown the space charge development in DBDs through theoretical and numerical studies [10–14]. Experimentally, Kozlov *et al.* [15] showed the local electric field and electron density by single MD employing a spatio-temporally resolved spectroscopy. However, the behavior of the space charge during the entire AC cycle has not been discovered in detail yet.

In this regard, we performed a two-dimensional (2D) visualization of the space charges in a pin-to-line geometry. To deduce the information of the space charges, we used an indirect method by measuring the electric field employing a laser-based electric field measurement technique (electric-field-induced second harmonic generation (EFISH) technique). The space charge distribution could be obtained mathematically using Gauss's law.

2. Experiment

Experimental setup including a DBD section are schematically illustrated in Fig. 1. To achieve MDs at a controlled position, a metallic pointy electrode and line electrode covered by a barrier were used. The pointy electrode was mounted on a Teflon frame, and the line electrode (4-mm thick and 130-mm long) was covered with α -Al₂O₃ ceramic (4-mm thick). A gas gap distance from the edge of the pointy electrode and the upper surface of the ceramic was set at 4 mm. No flow system and no confinement were applied to the DBD section.

A voltage amplifier (Trek, 30/20A), which amplified a signal from a function generator (NF, WF1974), supplied

AC high voltage (HV) of 4 kHz and 30 kV_{pp} (peak-to-peak) to the pointy electrode, while the line electrode was grounded. Applied HV (V_a) and the current were measured with a 1000:1 HV probe (Tektronix, P6015A) and a current monitor (Pearson, 6585). A monitoring capacitance to obtain a QV plot was installed between the line electrode and the ground terminal. A voltage across the monitoring capacitance was measured with a 10:1 voltage probe (Tektronix, TPP1000). An oscilloscope (Tektronix, DPO4104B) acquired the above signals.

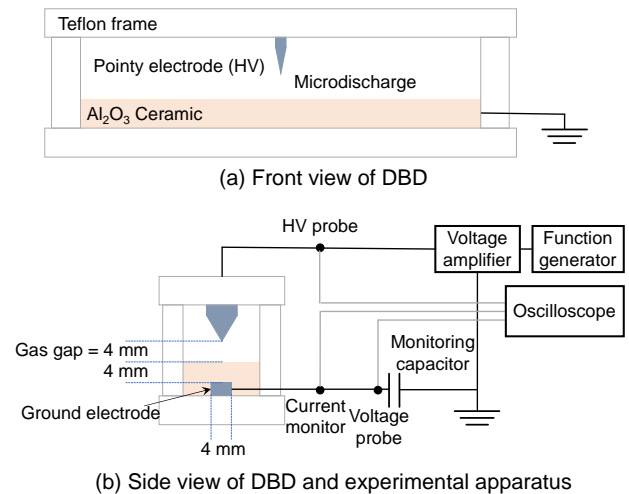


Fig. 1. Schematic of the experimental setup including a DBD section.

We employed EFISH technique to measure the electric field in the DBD section. The basic principle of EFISH is to use the generation of a second harmonic signal (SHG) when a laser beam is exposed to an electric field. The intensity of SHG ($I_{\lambda/2}$) is given by Eq (1):

$$I_{\lambda/2} \propto (I_{\lambda} E N)^2 \chi, \quad (1)$$

where I_{λ} is the intensity of the incident beam, E is the local electric field, N is the number density of scattering species, and χ is 3rd-order susceptibility. Although sometimes the signal needs to be calibrated if the dependencies of the EFISH signal on χ and N are significant [16], in this study χ and N were assumed to be constant. Thus, SHG was

considered proportional to the square of the electric field and the incident beam intensity.

The EFISH measurement system consisted of a picosecond Nd:YAG laser (Ekspla, PL2251A), a delay generator (BNC, Model 575), lenses, dichroic mirrors, a half-wave plate, a Long-Pass filter (LP), a prism, a photodiode (PD, Thorlabs, DET025A), and a photomultiplier tube (PMT, Hamamatsu, H10721-01), as shown in Fig. 2. The Nd:YAG laser provided a pulsed beam of ~ 15 mJ at 50 Hz. The delay generator controls the timing between the laser pulse and sinusoidal V_a . The incident beam delivered from the laser was polarized horizontally or vertically by the half-wave plate and then focused into the DBD section by the convex lens. Parasitic SHG, that may occur upstream before entering the DBD, was removed by the LP. The SHG generated in the DBD was spatially separated from the incident beam through a prism after being collimated by the convex lens. The incident beam and SHG were measured with PD and PMT, respectively.

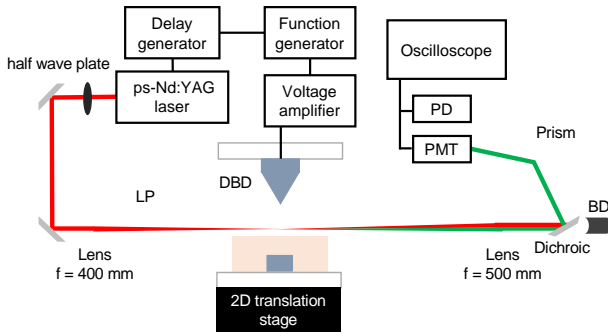


Fig. 2. EFISH measurement system.

Figure 3 shows a measuring domain in a x - z plane. The size of the domain was 10×4 mm², and a spatial resolution was 0.25 mm, resulting in a total of 654 points of measurement. Due to a practical limitation caused by a laser-wall interaction, a minimum distance from the ceramic surface was 0.25 mm.

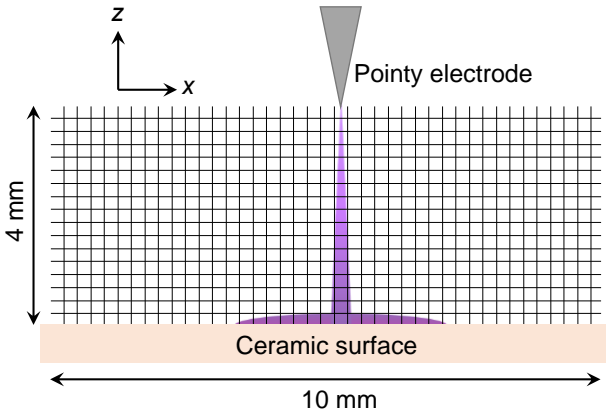


Fig. 3. Domain of EFISH measurement with a 0.25 mm measuring internal (10×4 mm², 654 total points).

3. Results and discussion

Two moments in the positive phase of V_a were of interest conditions. Figure 4 presents obtained QV plot with $V_a = 30$ kV_{pp}, and 4 kHz. During the positive phase V_a , four stepwise increments in charge appear. Each jump in the charge indicated a charge transfer by a single MD. The first measuring point represents a moment immediately after the end of the four consecutive MDs. The second measuring point was selected after 40 μ s from the first measurement to investigate the evolution of the space charge distribution.

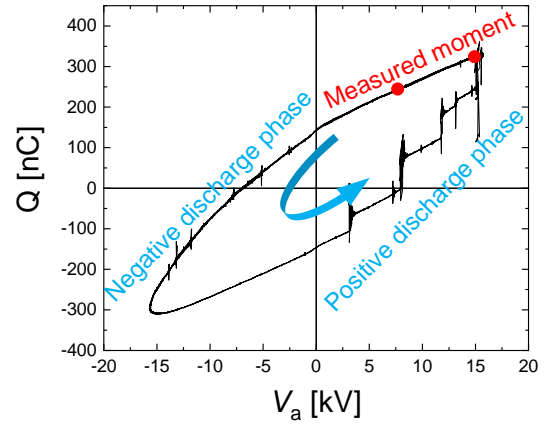


Fig. 4. QV plot with sinusoidal AC of 30 kV_{pp} and 4 kHz and measuring points after four consecutive MDs.

We used Gauss's law in Eq (2), to obtain the space charge from the measured electric field.

$$\frac{dE}{dx} = \frac{e}{\epsilon_0} n_c, \quad (2)$$

where $e = 1.60 \times 10^{-19}$ C, the elementary charge, $\epsilon_0 = 8.85 \times 10^{-12}$ F/m, the permittivity of free space, and n_c is a net space charge. To obtain an accurate value of the space charge, all changes in the electric field in the x , y , and z directions should be considered. However, here we presented only the electric field in the horizontal direction (E_x) because, as a result of the measurement, the change in the electric field in the vertical direction (z) was negligible compared to the horizontal direction. By analyzing the horizontal electric field, we were able to obtain a reasonable space charge distribution, although we could not quantify the space charges.

Figures 5 and 6 illustrate normalized horizontal electric field, E_x , and its change in x -direction, dE_x/dx . As explained above, dE_x/dx can be interpreted as the space charge distribution according to Gauss's law. For both measuring moments, E_x is almost zero due to symmetry at the center (*i.e.* $x = 0$ mm), and the field intensity increases as the measuring position becomes farther from the center. At the measuring point right after MDs, the field intensity reached a maximum around $x = 3$ mm (Fig. 4a). On the other hand, after 40 μ s, overall field intensity is lower and the contours

of the electric field in the central region is broader (Fig. 6a). Especially at the top ($z = 4$ mm), the contours of the electric field are noticeably broadened. The decay of the electric field can be well explained by the behavior of the space charge distribution. As shown in Fig. 5b, a column of space charge can be identified formed at the end of multiple MDs. Remarkably, the highest space charge density is seen near the tip of the pointy electrode and the dielectric surface. After $40 \mu\text{s}$, somewhat radially diffused space charges can be identified (Fig. 5b). Positive HV was still applied to the pointy electrode, so the downward electric field also pushed down the positive ions. Therefore, overall decayed space charge distribution could be observed.

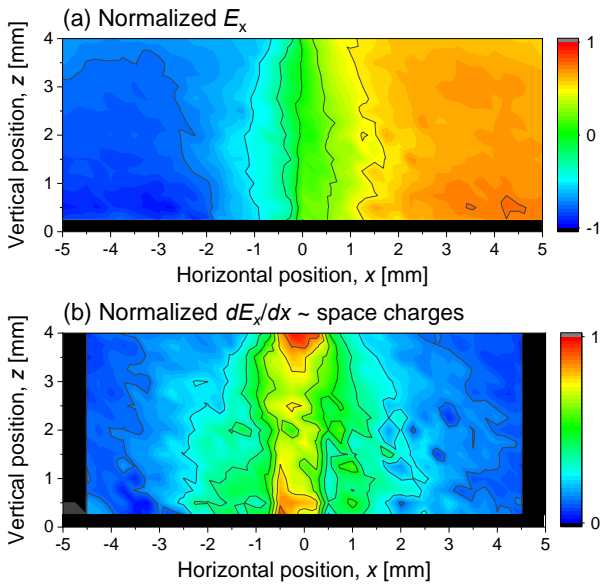


Fig. 5. Normalized horizontal electric field and space charge right after multiple MDs.

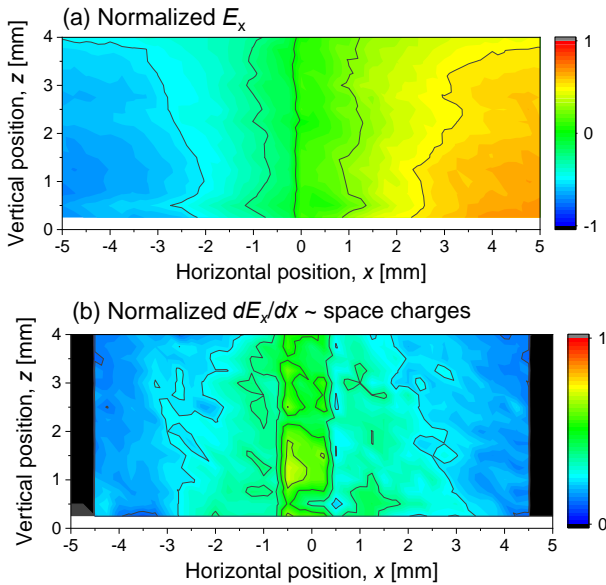


Fig. 6. Normalized horizontal electric field and space charge at $40 \mu\text{s}$ after the first measurement.

4. Conclusion

We measured the electric field using EFISH technique and obtained the space charge distribution from the Gauss's law in a pin-to-line type dielectric barrier discharge. The space charge formed by microdischarges appeared as a columnar shape, showing relatively denser distribution near both electrodes. As time elapsed, the space charges spread out due to a molecular and ambipolar diffusions.

Acknowledgments

The research reported in this publication was funded by King Abdullah University of Science and Technology (KAUST), under award number BAS/1/1384-01-01.

5. References

- [1] W. Siemann, *Annalen der Physik*, 178, 9 (1857).
- [2] D.S. Kim and Y.S. Park, *Journal of Environmental Science International*, 20, 5 (2011).
- [3] M. Kuraica, B. Obradović, D. Manojlović, D. Ostojić, and J. Purić, *Ind. Eng. Chem. Res.*, 45 (2006).
- [4] L. Vander Wielen, M. Östenson, P. Gatenholm, and A. J. Ragauskas, *Carbohydrate polymers*, 65, 2 (2006).
- [5] T. Shao, W. Yang, C. Zhang, Z. Niu, P. Yan, and E. Schamiloglu, *Applied Physics Letters*, 105, 7, (2014).
- [6] T. Shao, F. Liu, B. Hai, Y. Ma, R. Wang, and C. Ren, *IEEE transactions on Dielectrics and Electrical Insulation*, 24, 3 (2017).
- [7] H. Ayan, G. Fridman, A. F. Gutsol, V. N. Vasilets, A. Fridman, and G. Friedman, *IEEE transactions on plasma science*, 36, 2 (2008).
- [8] S. U. Kalghatgi, G. Fridman, M. Cooper, G. Nagaraj, M. Peddinghaus, M. Bal-asubramanian, V. N. Vasilets, A. F. Gutsol, A. Fridman, and G. Friedman, *IEEE transactions on plasma science*, 35, 5 (2007).
- [9] U. Kogelschatz, *Plasma Chem. Plasma Process*, 23, 1 (2003).
- [10] B. Eliasson, *IEEE transactions on plasma science*, 19, 2 (1991).
- [11] D. Braun, V. Bibalov, and G. Pietsch, *Plasma Sources Science and Technology*, 1, 3 (1992).
- [12] G. Steinle, D. Neundorf, W. Hiller, and M. Pietralla, *Journal of Physics D: Applied Physics*, 32, 12 (1999).
- [13] V. Gibalov and G. Pietsch, Siemens, *Journal of Physics D: Applied Physics*, 33, 20 (2000).
- [14] Y. Akishev, G. Aponin, A. Balakirev, M. Grushin, V. Karalnik, A. Petryakov and N. Trushkin, *Plasma Sources Science and Technology*, 20, 2 (2011).
- [15] K. Kozlov, H-E. Wagner, R. Brandenburg and P. Michel, *Journal of Physics D: Applied Physics*, 34, 21 (2001).
- [16] T. Butterworth and M.S. Cha, *Proceedings of the Combustion Institute*, 38, 4 (2021).